scientific reports

OPEN

Carbonization and H$_3$PO$_4$ activation of fern *Dicranopteris linearis* and electrochemical properties for electric double layer capacitor electrode

Trang K. Trinh[1], Toshiki Tsubota[1✉], Shuto Takahashi[1], Nga T. Mai[2,3], Minh N. Nguyen[3✉] & Nam H. Nguyen[4]

Today, the world's climate change is a growing problem, plant carbon sequestration is one of the effective ways to mitigate climate change by reducing greenhouse gases, mostly carbon gases. *Dicranopteris linearis* (*D. linearis*), a common fern species in the tropic or subtropic ecoregions, has been recently recognized as a potential feedstock to produce highly porous biochar. This study aims to enhance the specific surface area (SSA) and pore volumes of biochars derived from the *D. linearis* by H$_3$PO$_4$ activation and examine electrical properties of the activated biochars and their possible usage for the electric double-layer capacitor (EDLC) electrode. The treated raw fern was activated with H$_3$PO$_4$ 85% by the three different mixing ratios 1:0, 1:1, and 1:3 (w/w) and then pyrolysis under N$_2$ flow maintained at 500 °C for 1 h. The performance as the electrode for an EDLC was evaluated in 1 mol L^{-1} H$_2$SO$_4$ solution for the H$_3$PO$_4$-activated samples. The SSA and pore volumes were drastically increased after activation. The maximum SSA and pore volume were 1212 m^2 g^{-1} and 1.43 cm^3 g^{-1}, respectively for the biochar activated at 400 °C with a weight mixing ratio 1:3 (w/w) between the fern and H$_3$PO$_4$ acid while these values of the biochar at 400 °C were 12 m^2 g^{-1} and 0.02 cm^3 g^{-1}, respectively. The biochar activated at 600 °C with the mixing ratio 1:1 (w/w) showed the maximum capacitance value, *ca*. 108 F g^{-1} at 1 mV s^{-1}. The activation using H$_3$PO$_4$ showed a positive tendency to enhance electrochemical properties and it could be a premise toward a higher performance of EDLC from the *D. linearis* derived activated biochar.

Today, the world's climate change is a growing problem, increasing ocean depth, changing plant and animal habitats, and making storm stronger and more dangerous[1]. Climate change is caused by greenhouse gases, mostly carbon gases that build up in our atmosphere trapping the heat from the sun and stopping it from escaping into space. Carbon gases such CO$_2$ and CO are mainly released when people use fossil fuels such as gas diesel and coal. It is important to take carbon out of the air to reduce the impact of greenhouse effects. The process of removing carbon from the air and storing is called carbon sequestration. One effective and natural method of carbon sequestration that tree suck in carbon and converted into wood which they bury deep underground in the form of roots which can be turn into charcoal by controlled or naturally burns. However, one major challenge of using biomass as an energy carrier is the treatment of such emissions during the thermal process (combustion/pyrolysis). Nitrogen oxides (NOx), are considered one of the main gas emissions during the thermal processes of biomass and NOx family gases are often recognized to cause acid rain[2]. Therefore, these kinds of emissions need to be controlled to reduce their impact on the environment and human health[3]. Hence, there are more and

[1]Department of Materials Science, Faculty of Engineering, Kyushu Institute of Technology, 1-1 Sensuicho, Tobata-ku, Kitakyushu, Fukuoka 804-8550, Japan. [2]Faculty of Environmental and Natural Resources, Ha Tay Community College, Thuy Xuan Tien Ward, Chuong My District, Hanoi, Vietnam. [3]Faculty of Environmental Sciences, University of Science, Vietnam National University, Hanoi (VNU), 334 Nguyen Trai, Thanh Xuan, Hanoi, Vietnam. [4]Energy Department, University of Science and Technology of Hanoi, Vietnam Academy of Science and Technology, 18 Hoang Quoc Viet Street, Cau Giay District, Hanoi, Vietnam. ✉email: tsubota@che.kyutech.ac.jp; minhnn@vnu.edu.vn

more researchers use biomass as a precursor material for producing biochars or activated biochars in controlled conditions.

Fern *Dicranopteris linearis* (*D. linearis*) is known as one of the most serious weed species due to their wide-spread from tropical to subtropical ecoregions[4]. Nevertheless, their economic value has received little attention. In many remote regions, this fern is burned to fertile soils (slash-and-burn agriculture) or used as a material for covering soil surface or earlier it has been an important fuel for local minorities. More recently, *D. linearis* has been more intensively studied and the findings suggested this fern species as a potential material for biochar production[5] or soil improvement[6,7]. This encourages more research works to get the advantages from this type of species economically and efficiently[5–10].

Activated carbon has a wide range of applications in reality such as medicine, industry, agriculture, and the environment due to its ability of adsorption and desorption. Activated carbon is known as purified charcoal, treated physically or chemically to generated micro-fissures that vastly increase its SSA, thereby enhancing exposure for adsorption or chemical reactions[11]. Chemical activation usually provides activated carbon with higher SSA than that of activated carbon prepared by physical activation. Chemical substance as phosphoric acid (H_3PO_4) is a highly recommended activator for the preparation of activated carbon due to its benefits of relatively lower activation temperature than other typical alkali activators such as KOH, K_2CO_3, NaOH, etc. For example, Hayashi et al., reported that in comparison with other alkali activators, H_3PO_4 allowed to obtain the high SSA ($>1000\ m^2\ g^{-1}$) and total pore volumes at the lower temperature range (400–600 °C) while the effective temperature for alkali activators was 800 °C[12]. The lower temperature activation means safer, more economical, and more convenient for practical uses. Moreover, H_3PO_4 has a relatively lower toxicity than other common activators such as $ZnCl_2$ and KOH. Many researchers have paid attention to H_3PO_4 activation to enhance SSA and total pore volumes of their carbon material[12–18]. Abdenaeim and De Yuso reported that the main mechanisms of activation with phosphoric acid are the depolymerization, dehydration and redistribution of biopolymers in lignocellulosic materials[19,20] to created tunnel-shaped and generally have a honeycomb structure on the surface of activated carbon[21,22]. Activated carbon with large SSA and suitable pore size, which also leads to high electrical conductivity and enhance the performance of the electric double-layer capacitor (EDLC) electrode, a well-known electric power storage device nowadays[23–25].

The electric power storage in EDLC is performed by utilizing the interlayer between electrode surfaces and electrolytes. So far, many kinds of agricultural wastes such as pine cones, coconuts shells, rice husk[26], strobili fibers[27], durian shells[28], bamboos[29], starch[30] and flowers[31] have been investigated as promising raw materials to create activated carbon for the EDLC electrode. Having higher SSA in comparison with other biochar prepared at the same pyrolysis condition[5], fern *D. linearis* can also be a promising material to prepared activated biochar and use for the EDLC electrode. This study evaluated the performance of H_3PO_4 in activating fern *D. linearis* derived biochars, electrical properties of the activated biochars and the feasibility of using these activated materials for well-performed EDLC electrodes.

Material and methods

Material and sample preparation.

Production of biochars. The fern *D. linearis* was collected in a hilly area at Pho Yen district, Thai Nguyen province, Vietnam (Long: 105.485° E; Lat: 22.762° N) was air-dried, chopped into small segments (size ~ 1 mm) and then kept in the dried and clean plastic bottles for further investigation. Detailed description of the heat treatment apparatus used in this study is shown in Supplementary Fig. S1 online. Pyrolysis of the *D. linearis* biomass was conducted under N_2-supported at three different temperatures, i.e., 400, 600 and 800 °C in an oven (Nabertherm LT 24/12/P300). For each experiment, approximately 300 g of D. *linearis* was put into an airtight steel box (10 cm in height and 20 cm in diameter). The pyrolysis process was installed at a heating rate of 15 °C min^{-1} with N_2 supporting at 3 NL min^{-1} (NL: Normal litter at 273 K and 1 atm) and maintained for 1 h.

Activation procedure. For activation, each 60 g of D. *linearis* biomass was mixed with H_3PO_4 (85%) by the mixing ratio 1:0, 1:1, and 1:3 (w/w) in an airtight refractory steel box 25 cm in diameter and 20 cm in height and put in an electric muffle furnace (Nabertherm LT 24/12/P300). The pyrolysis process was installed at a heating rate of 15 °C min^{-1} with N_2 supporting at 3 NL min^{-1} (NL: Normal litter at 273 K and 1 atm) and maintained at 500 °C for 1 h.

Characterizations.

Chemical composition of *D. linearis* biomass was examined by executing wet digestion with aqua regia solution and then dissolved Si was determined by molybdate blue method while other dissolved ions were analyzed by inductively coupled plasma mass spectrometry (ICP-MS, Agilent 7900). The micro-structures of the samples were observed by scanning electron microscope (SEM, JEM5310, JEOL). To characterize the SSA and pore volumes, N_2 adsorption isotherms and CO_2 adsorption isotherms were measured by a commercial apparatus (BELSORP mini II, MicrotracBEL Corporation instrument). The data of N_2 adsorption isotherms were used for the estimation of Barrett–Brunauer–Emmett–Teller (BET) SSA, total pore volume, and micro-pore volume by using the *t*-plot statistical thickness method. CO_2 adsorption isotherms were used for the estimation of micro-pore volume by using Dubinin–Astakhov (DA) method. To understand the properties of the samples, several methods were conducted such as CHN measurement (CHN corder MT-5, Yanako), XRF measurement (S8 TIGER, Bruker), and ^{13}C NMR measurement (JNM-ECX400, JEOL) for understanding the kind of elements in the samples. The measurement conditions of ^{13}C NMR were as follows, DEPTH2, CPMAS probe: 3.2 mm, MAS (Magic Angle Spinning) speed: 15 kHz. Moreover, FT-IR (Nicolet 6700, Thermo scientific) (ATR method) and XPS (AXIS-NOVA, Shimadzu/KRATOS) for defining the chemicals bonds and functional groups.

Electrochemical properties. Evaluation of the electrochemical performance as an electrode of electric double-layer capacitor was performed following the procedure suggested by Tsubota et al.[29–34]. The activated biochars were mixed with polytetrafluoroethylene (PTFE) and acetylene black (AB) by the mixing ratio 8:1:1 (w/w/w). PTFE played a role as a binder, while acetylene black (AB) acted as conductive agent. The mixtures were rolled to *ca*. 0.5 mm thickness, and then were cut into the rectangle shape 20 mm × 8 mm samples. The sheet samples were set on a Pt plate for collecting electrode, and a three-electrode cell was prepared for the electrochemical measurements. A 1 M H_2SO_4 aqueous solution, a Pt plate, and an Ag/AgCl electrode were used as electrolyte, a counter electrode, and reference electrode, respectively. The electrochemical measurements, such as cyclic voltammetry (CV) and galvanostatic charge–discharge measurement, were performed for the evaluation of electrochemical performance.

Results and discussion

Raw material. The elements in raw fern D. *linearis* were shown in Supplementary Fig. S2 online. The result shown that K, Na, Ca, Al, Si are the main inorganic elements in the chemical composition of the D. linearis fern. Alkaline metal (K, Na) and alkaline-earth metal (Ca, Mg) were main elements, but Al and Si also existed in the fern. All toxic heavy metals as Cr, Ni, As, Cd, Hg, Pb, etc. did not appear so this demonstrated the purity of raw material.

Characteristics of biochars and activated biochars. The SEM (Fig. 1) images of the carbonized samples indicated that the sizes of the particles, which had the micro-structure derived from plant issues, were independent of the carbonization temperature. Therefore, the structure of raw material was not destroyed by the carbonization at the temperature region (400–800 °C).

The N_2 adsorption isotherms at 77 K of the carbonized samples are shown in Fig. 2. The adsorbed volumes of the sample carbonized at 400 °C were relatively low, while these volumes of biochars obtained at 600 °C and 800 °C were obviously higher; and increased rapidly in the region of the low relative pressure. In addition, the curves of all samples did not close in the low-pressure region, which was considered as low-pressure hysteresis. The low-pressure hysteresis appeared when the diameters of pores were near to the size of nitrogen molecule (approximate 0.35 nm). The difference between adsorption isotherm and desorption isotherm at low pressure decreased when the pyrolysis temperatures increased.

The CO_2 adsorption isotherms at 298 K of the carbonized samples are shown in Supplementary Fig. S3 online. The patterns of the adsorbed volumes obtained from the biochars carbonized at 600 °C and 800 °C were similar. These volumes are much larger than that volume of the 400 °C sample. The drastic increment of the adsorbed volumes from 400 to 600 °C means that the volume of pore less than 0.7 nm in diameter classified as ultra-micropores largely increased from 400 to 600 °C. The chemical reactions for carbonization, such as pyrolysis, generate gaseous species leading to the formation of ultra-micropores progress in the region from 400 to 600 °C; and the irradiations of these gases increased significantly from 400 to 600 °C. The slight increment of adsorbed volumes from 600 to 800 °C could be reasonable due to the carbonization reactions which generate gaseous molecules until 600 °C.

The values related to SSA and pore volume estimated from N_2 adsorption isotherms and CO_2 adsorption isotherms are listed in Table 1. The BET SSA (S_{BET}), total pore volume (V_{total}), and micropore volume (V_{micro}) estimated from CO_2 adsorption isotherms by Dubinin-Astakhov (DA) model increased with increasing the carbonization temperature. The index number of DA models depends on the pyrolysis temperature and relates to the pore size distribution, so pyrolysis temperatures should affect the pore size distribution of the samples. The change in SSA and the pore conditions such as pore volumes and pore size distribution of the samples as the follows.

- At 400 °C, pores were poorly generated. Most of the pores had very small diameters, which cause low-pressure hysteresis at N_2 adsorption isotherm.
- At 600 °C, relatively many pores were created by the irradiation of gaseous molecules derived during the pyrolysis processes. Therefore, the volume of ultra-micropore and micropore significantly increased for both N_2 and CO_2 adsorption isotherms when pyrolysis temperature changed from 400 to 600 °C.
- At 800 °C, the diameter of pores increased, which was explained by the increase of the N_2 adsorbed volumes from 600 to 800 °C as shown in Fig. 2. The N_2 adsorbed volumes at 800 °C were about two times higher than the value at 600 °C, while in CO_2 adsorption isotherm these values were similar at both temperatures. The larger molecules are diffused into the larger pores on the sample surfaces, so the discrepancy of N_2 adsorbed volumes at 800 °C and 600 °C indicated the difference of pore size. In that case, samples prepared at 800 °C has larger pore size compare to others.

The contents of C, H and N are listed in Table 2. The ash content was 9.74 wt.%. The XRF result illustrated that the ash contents of the sample mainly consist of K, Ca, Si, and Al in Table 3. In comparison with the chemical components of raw material, Na no longer appeared in the biochar samples. That means Na elements were removed during the pyrolysis process. Nguyen et al.[35] reported that the relationship of pyrolysis temperature and potassium (K) which element has the highest percentage in the XRF detection. From XPS data Nguyen et al. found that the intensities of the peaks related to K decreased with increasing the heating temperature and disappeared at 800 °C so the K atoms changed to higher valence at 600 °C[35].
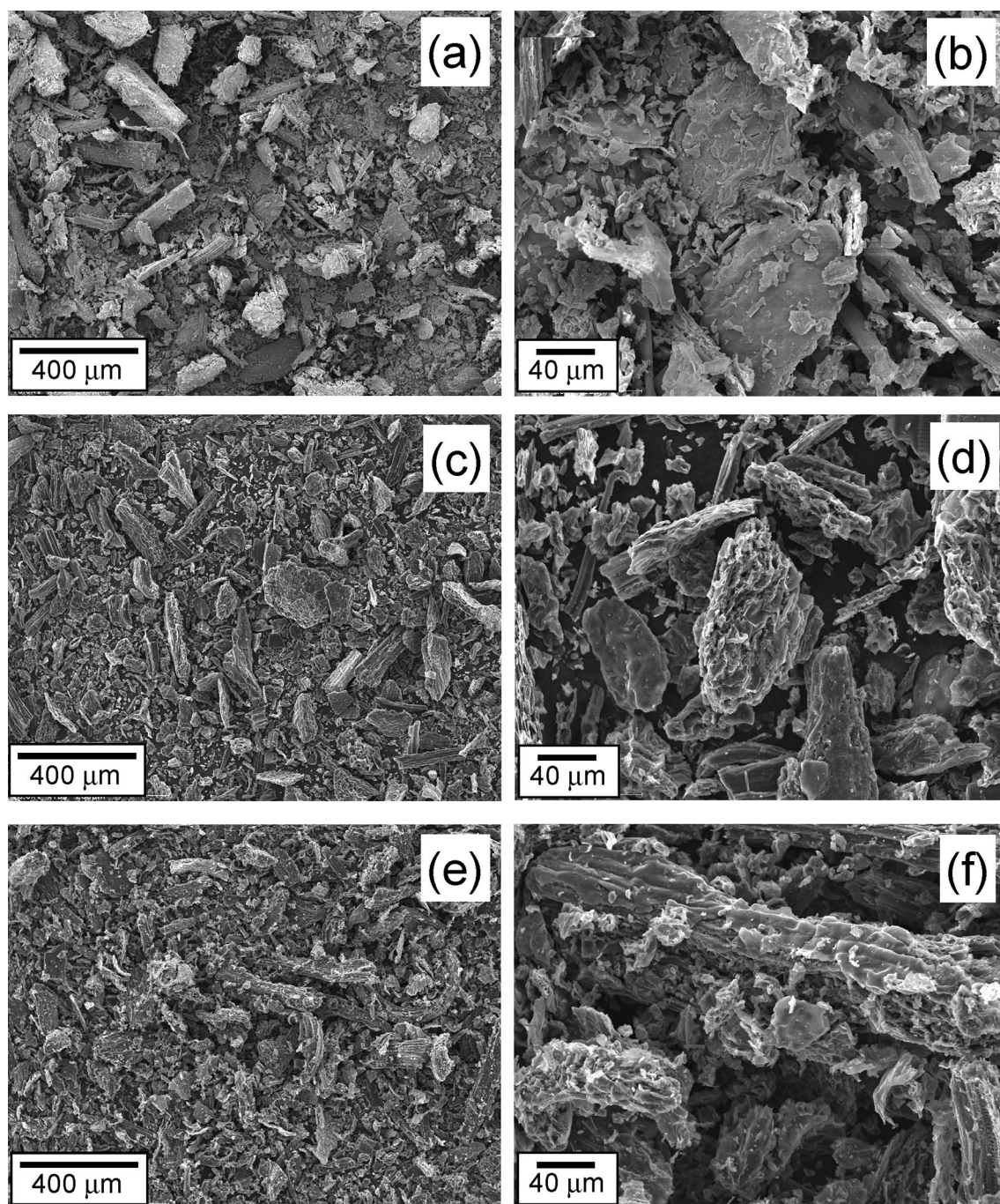
Figure 1. SEM images of the samples. (**a**,**b**) Carbonized at 400 °C, (**c**,**d**) Carbonized at 400 °C, (**e**,**f**) Carbonized at 400 °C.

H_3PO_4 activation. The SEM images (see Supplementary Fig. S4 online) indicated the micro-structure of the H_3PO_4-activated biochars in which the particles were independent of the activation condition such as temperature and the amount of added H_3PO_4. Some parts of the activated biochars were likely slagged leading to smoother surface and unified pores.

The N_2 adsorption isotherms of the activated samples are shown in Fig. 3. The adsorbed volume increased with the increasing amount of H_3PO_4 and decreased with increasing the heating temperature. When the mixing ratio of H_3PO_4 to raw material was 3, the adsorbed volume rapidly increased with the relative pressure (p/p_0) higher than 0.8. Because the size distributions of the activated biochars were similar each other, the origin of the rapid increment was defined by the increase of N_2 diffusion not into the interparticle void but into the pores on particles. Luo et al. also reported[17] that the SSA and total pore volume dramatically increased with the mixing ratio 1:3 (w/w), and then decreased in the higher mixing ratio. The reason for the decrement was presumed by Luo et al.[17] that higher concentration of H_3PO_4 forms some phosphorus compounds which blocked the porosity
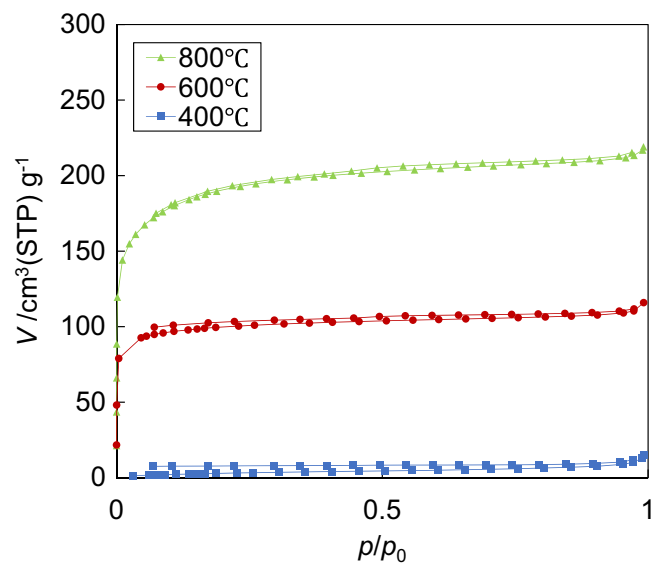
Figure 2. N_2 adsorption isotherms of the samples.

	S_{BET} (m² g⁻¹)	V_{total} (cm³ g⁻¹)	V_{micro}(DA) (cm³ g⁻¹)	Index number (of DA)
400 ℃	12	0.02	0.13	2.3
600 ℃	387	0.18	0.27	1.9
800 ℃	702	0.34	0.39	1.7

Table 1. The values estimated from adsorption isotherms.

Element	wt.%
C	75.61
H	2.34
N	1.50
Residue	9.74
Others	10.81

Table 2. CHN measurement for G600.

Element	wt.%
K	31.41
Ca	27.44
Si	20.88
Al	8.84
P	3.19
Fe	2.64
Mg	1.89
Mn	1.52
S	1.20
Cl	0.99

Table 3. XRF result for G600.
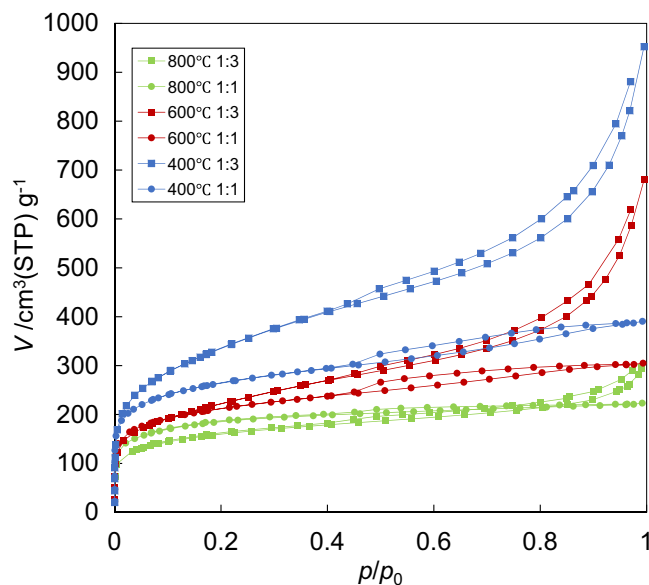
Figure 3. N_2 adsorption isotherms of the samples activated with H_3PO_4.

H_3PO_4 activation	S_{BET} (m² g⁻¹)	V_{total} (cm³ g⁻¹)	V_{micro} (cm³ g⁻¹)	V_{meso} (cm³ g⁻¹)	V_{micro}(DA) (cm³ g⁻¹)	Index number (of DA)
400 °C 1:1	944	0.60	0.39	0.31	0.42	1.7
400 °C 1:3	1212	1.43	1.32	1.20	0.58	1.4
600 °C 1:1	758	0.47	0.47	0.24	0.34	1.7
600 °C 1:3	761	0.92	0.90	0.78	0.38	1.5
800 °C 1:1	660	0.35	0.34	0.11	0.32	1.7
800 °C 1:3	570	0.46	0.39	0.28	0.24	1.7

Table 4. The values estimated from adsorption isotherms for the samples activated with H_3PO_4.

of activated carbon. The N_2 adsorption isotherms for H_3PO_4 activation reported by Luo et al.[17] and by Hayashi et al.[12] were different from those of this study. They reported that pore volume and SSA decreased with increasing the activation temperature at > 600 °C while this study showed the highest values at 600 °C and then decreased at the higher pyrolysis temperatures. The differences in pretreatment processes and raw biomass sources were the reasons for the distinctive results. Figure 3 showed the hysteresis loop which closed around 0.4 of p/p_0 explained by the theory based on capillary condensation in pores. Because capillary condensation can occur in mesopore (2–50 nm), these samples should have mesopores.

The CO_2 adsorption isotherms at 298 K are shown in Supplementary Fig. S5 online. The adsorbed CO_2 volume decreased with increasing the added H_3PO_4 amount. Because the adsorbed CO_2 volume should be related to ultra-micropore (< 0.7 nm in diameter), the decrease of the adsorbed volume should mean the reduction of the volume for very small pores such as ultra-micropore of the sample. One of the reasons lead to the decrements is the expansion of pore sizes (larger than CO_2 molecule) due to the superimposing of ultra-micropores in the biochars activated by adding a higher H_3PO_4 amount.

The values related to SSA and pore volumes were estimated these adsorption isotherms and were listed in Table 4. The curves in Fig. 3 represent type IV adsorption isotherm. The vertical increment at the near-zero of relative pressures should indicate the existence of micropores. Because all the values of V_{micro} were estimated from N_2 adsorption isotherms by using the t-plot theory, the estimated pore volume roughly assigned to 0.7–2.0 nm in diameter. V_{micro} (DA) was estimated from CO_2 adsorption isotherm with extrapolation. V_{meso} was estimated from N_2 adsorption isotherm by using the BJH theory. The sample with the mixing ratio 1:3 (w/w) prepared at 400 °C had the largest S_{BET} value (1212 m² g⁻¹) and all the volumes. In comparison with other biomass sources in Supplementary Table S1 online, the S_{BET} of D. *linearis* activated biochar is similar while V_{total} and V_{micro} are higher than most of others[15,16,28,36–42]. Therefore, fern D. *linearis* derived activated carbon with both micro and mesopores could be effectively prepared by H_3PO_4 activation.

It is obvious from the experimental results of N_2 and CO_2 adsorption isotherms listed in Tables 1 and 4 that both SSA and total pore volume were significantly enhanced by H_3PO_4 activation. Processes that occurred during activation with H_3PO_4 acid were the cellulose depolymerization, biopolymers dehydration, and redistribution of biopolymers in biomass[43,44], which enhanced the total pore volumes and SSA. The H_3PO_4 added in the raw material acted as the catalyst for the cleavage of cellulose fibers and cross-links in the biomass shell to formation of gases, volatile fragments and soluble products during the activation processes[28,44,45]. In Supplementary Table S2
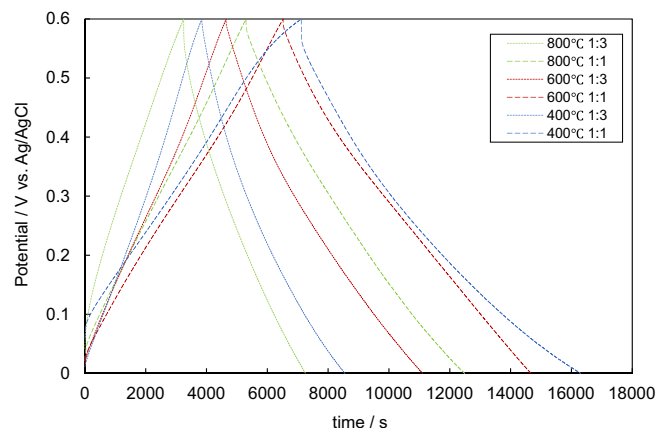
Figure 4. The graphs of charge–discharge measurement at 10 mA g^{-1} of the samples activated with H$_3$PO$_4$.

online, The C contents of the samples prepared by H$_3$PO$_4$ activation were lower than those of the samples that were simply prepared by carbonization, while the other remaining compounds increased with increasing the amount of added H$_3$PO$_4$. The reason could be presumed that the appearance of some inorganic compounds generated during H$_3$PO$_4$ activation such as polyphosphoric acid. The XPS (in Supplementary Fig. S6 online) demonstrated the intensive of others element like N, P, Si, etc., increase with the increase of temperature and the H$_3$PO$_4$ amount. ^{13}C NMR graphs shown in the Supplementary Fig. S7 online has been shown that the activated carbon prepared with phosphoric acid has less C=O groups than the raw materials. The reduction of carbonyl groups may be due to the effect of H$_3$PO$_4$ hydrolysis, which decomposes these groups and other products such as volatile substances[46]. The FT-IR chart show (Supplementary Fig. S8 online) that the transmittance of O–H and C=O group decrease with the increase of temperature and H$_3$PO$_4$ doses. These experimental results indicate that the addition of H$_3$PO$_4$ affects the functional groups in biochar.

Electrochemical properties. The results of cyclic voltammetry (CV) (scan rate: 1 mV s^{-1}) are shown in Supplementary Fig. S9 online. The larger area of CV graph indicates the capacitance value, and the like-rectangular shapes of CV graph show the capacitance derived from electric double layer. Therefore, the large area with rectangular shape of CV graph means the high performance of electrochemical properties of the sample. When the activation temperature was 600 °C, the CV graph of the sample tended to a larger area than that of others. The trend of the activated sample prepared at 600 °C were relatively rectangular although some peaks were still observed. Despite having larger SSA and pore volumes, the activated carbons prepared at 400 °C revealed their smaller areas of CV charts as compare to the 600 °C activated samples. In general, electrical conductivity depends on the treated temperature. The electrical conductivity of carbonized samples drastically increases from about 800 to c.a. 1000 °C. Electrical conductivity is one of the important factors which affect the capacitance values. At lower treated temperature (e.g., 400 °C) can be the reason why activated carbons at 400 °C has low capacitance while its SSA is the highest.

The pyrolysis temperatures dependence of the capacitance values at 1 mV s^{-1} are shown in Supplementary Fig. S10 online. The samples prepared with the mixing ratio 1:1 (w/w) had the higher capacitance values than the samples prepared with the mixing ratio 1:3 at all carbonization temperature. It was likely that H$_3$PO$_4$ activation were effective at the low impregnation ratio for large capacitance value. The presumed reason could be excessive phosphoric acids reacted more with organic compounds in the precursor leading to the formation of phosphate and polyphosphate bridge and esters linkage with OH$^-$ group at cellulose[44] as electrical insulating layers. The sample prepared at 600 °C with the mixing ratio 1:1 (w/w) had the highest value of capacitance about 110 F g^{-1} (scan rate 1 mV s^{-1}). The capacitance values are higher than the previously reported values such as 82.5 F g^{-1} (scan rate: 50 mV s^{-1}) and 72 F g^{-1} (scan rate: 200 mV s^{-1}) of activated biochar derived from durian prepared by H$_3$PO$_4$ activation[28]. However, the activated carbons prepared in this study was not considered as high electrochemical performances because the capacitance value per weight estimated by two-electrode cell is 1/4 times in comparison with 3-electrode system.

The patterns of charge–discharge measurement at 10 mA g^{-1} are shown in Fig. 4. The shapes of these graphs were nearly isosceles triangles indicating that the electric energy was stored not by redox reactions but by the electric double layer. The shape type of charge and discharge curve is usually obtained from the carbon-based electrode EDLC[28,31]. Therefore, the samples in the cells act as the active material of EDLC.

The capacitance values calculated from the results of charge–discharge measurements are shown in Supplementary Fig. S11 online. Recent studies have reported the capacitance values which were measured in the electrolyte of 1 M H$_2$SO$_4$ aqueous solution[31,47,48]. One of the reasons for lower capacitance values at higher current densities could be the low electrical conductivity of the activated samples. Moreover, the lower capacitance values also attributed to insufficient electrolyte ions diffusion kinetics across the micropores. The reduced accumulation amount of electrolyte ions onto porous electrode interfaced results of the reduction in specific capacitance[31]. The specific capacitance values of all the activated biochars of this study nearly closed to 0 at 1000 mA g^{-1}, which is not

suitable as an EDLC electrode. Chang et al.[31] reported an effective result that the capacitance value of 211.6 F g^{-1} could remain at 10,000 mA g^{-1}, revealing that the large capacitance value at high current density region. In spite that some of the activated biochars in the study had mesopores, the capacitance values of the samples were still low at high current density regions. The explanation is low electrical conductivity of the carbonized structure and to exist electrical insulators formed by the components generated during activation like polyphosphoric acid, oxides, and oxygen-containing functional groups as Molina-Sabio and Rodríguez-Reinoso recorded in his study[44]. Reducing the electrical resistance or remove the insulators layers is effective to improve the performance of EDLC electrodes, which might be interesting idea for future studies.

Conclusions

The present work focused on developing the SSA and total pore volume of biochar derived from fern D. *linearis* by H$_3$PO$_4$ activation and check the possibility of electrochemical performance for EDLC electrodes. All the N$_2$ adsorption isotherms for the biochars prepared at 400–800 °C showed low-pressure hysteresis, which indicates the existence of ultra-micropores. Dominant elements in the sample carbonized at 600 °C were potassium and calcium except for the elements related to organic compounds, such as carbon, oxygen, hydrogen. The activation by H$_3$PO$_4$ was effective for enhancing both the SSA and pore volume. The sample activated at 400 °C with the mixing ratio 1:3 (w/w) had the maximum values. The maximum capacitance value was ca. 108 F g^{-1} at 1 mV s^{-1} for the sample activated at 600 °C with the mixing ratio 1:1 (w/w) at the weight. The research opened an idea of a new research about suppression of electrical resistance to improve of the electrochemical performance.

References

1. Fawzy, S., Osman, A. I., Doran, J. & Rooney, D. W. Strategies for mitigation of climate change: A review. *Environ. Chem. Lett.* https://doi.org/10.1007/s10311-020-01059-w (2020).
2. Forbes, E., Easson, D., Lyons, G. & Mcroberts, W. Physico-chemical characteristics of eight different biomass fuels and comparison of combustion and emission results in a small scale multi-fuel boiler. *Energy Convers. Manage.* **87**, 1162–1169. https://doi.org/10.1016/j.enconman.2014.06.063 (2014).
3. Osman, A. I. Mass spectrometry study of lignocellulosic biomass combustion and pyrolysis with NOx removal. *Renew. Energy* **146**, 484–496. https://doi.org/10.1016/j.renene.2019.06.155 (2020).
4. Tet-Vun, C. & Ismail, B. S. Field evidence of the allelopathic properties of *Dicranopteris linearis*. *Weed Biol. Manag.* **6**(2), 59–67. https://doi.org/10.1111/j.1445-6664.2006.00203.x (2006).
5. Mai, N. T. *et al.* Fern *Dicranopteris linearis*-derived biochars: Adjusting surface properties by direct processing of the silica phase. *Colloids Surf. A* **583**, 123937. https://doi.org/10.1016/j.colsurfa.2019.123937 (2019).
6. Nguyen, M. N. *et al.* Fern, *Dicranopteris linearis*, derived phytoliths in soil: Morphotypes, solubility and content in relation to soil properties. *Eur. J. Soil Sci.* **70**(3), 507–517. https://doi.org/10.1111/ejss.12754 (2019).
7. Tran, C. T. *et al.* Phytolith-associated potassium in fern: Characterization, dissolution properties and implications for slash-and-burn agriculture. *Soil Use Manag.* **34**(1), 28–36. https://doi.org/10.1111/sum.12409 (2018).
8. Zakaria, Z. A. *et al.* Antinociceptive, anti-inflammatory, and antipyretic properties of an aqueous extract of *Dicranopteris linearis* leaves in experimental animal models. *J. Nat. Med.* **62**(2), 179–187. https://doi.org/10.1007/s11418-007-0224-x (2008).
9. Russell, A. E., Raich, J. W. & Vitousek, P. M. The ecology of the climbing fern *Dicranopteris linearis* on windward Mauna Loa, Hawaii. *J. Ecol.* **86**(5), 765–779. https://doi.org/10.1046/j.1365-2745.1998.8650765.x (2003).
10. Kamisan, F. H. *et al.* Effect of methanol extract of *Dicranopteris linearis* against carbon tetrachloride-induced acute liver injury in rats. *BMC Complement. Alternative Med.* **14**(1), 123. https://doi.org/10.1186/1472-6882-14-123 (2014).
11. Johnson, C. Advances in pretreatment and clarification technologies. *Comprehensive Water Qual. Purif.* **2**, 60–74. https://doi.org/10.1016/B978-0-12-382182-9.00029-3 (2014).
12. Hayashi, J., Kazehaya, A., Muroyama, K. & Watkinson, A. Preparation of activated carbon from lignin by chemical activation. *Carbon* **38**(13), 1873–1878. https://doi.org/10.1016/S0008-6223(00)00027-0 (2000).
13. Gao, Y. *et al.* Preparation of high surface area-activated carbon from lignin of papermaking black liquor by KOH activation for Ni(II) adsorption. *Chem. Eng. J.* **217**, 345–353. https://doi.org/10.1016/j.cej.2012.09.038 (2013).
14. Myglovets, M. *et al.* Preparation of carbon adsorbents from lignosulfonate by phosphoric acid activation for the adsorption of metal ions. *Carbon* **80**, 771–783. https://doi.org/10.1016/j.carbon.2014.09.032 (2014).
15. Liu, Q., Zheng, T., Wang, P. & Guo, L. Preparation and characterization of activated carbon from bamboo by microwave-induced phosphoric acid activation. *Ind. Crops Prod.* **31**(2), 233–238. https://doi.org/10.1016/j.indcrop.2009.10.011 (2010).
16. Yakout, S. & El-Deen, G. S. Characterization of activated carbon prepared by phosphoric acid activation of olive stones. *Arab. J. Chem.* **9**, S1155–S1162. https://doi.org/10.1016/j.arabjc.2011.12.002 (2016).
17. Luo, Y. *et al.* The performance of phosphoric acid in the preparation of activated carbon-containing phosphorus species from rice husk residue. *J. Mater. Sci.* **54**(6), 5008–5021. https://doi.org/10.1007/s10853-018-03220-x (2018).
18. Sun, Y., Yang, G., Zhang, J., Wang, Y. & Yao, M. Activated carbon preparation from lignin by H$_3$PO$_4$ activation and its application to gas separation. *Chem. Eng. Technol.* **35**(2), 309–316. https://doi.org/10.1002/ceat.201100309 (2011).
19. Abdelnaeim, M. Y., Sherif, I. Y., Attia, A. A., Fathy, N. A. & El-Shahat, M. Impact of chemical activation on the adsorption performance of common reed towards Cu(II) and Cd(II). *Int. J. Mineral Process.* **157**, 80–88. https://doi.org/10.1016/j.minpro.2016.09.013 (2016).
20. Yuso, A. M., Rubio, B. & Izquierdo, M. T. Influence of activation atmosphere used in the chemical activation of almond shell on the characteristics and adsorption performance of activated carbons. *Fuel Process. Technol.* **119**, 74–80. https://doi.org/10.1016/j.fuproc.2013.10.024 (2014).
21. Yorgun, S. & Yıldız, D. Preparation and characterization of activated carbons from Paulownia wood by chemical activation with H$_3$PO$_4$. *J. Taiwan Inst. Chem. Eng.* **53**, 122–131. https://doi.org/10.1016/j.jtice.2015.02.032 (2015).
22. Yorgun, S., Yıldız, D. & Şimşek, Y. E. Activated carbon from paulownia wood: Yields of chemical activation stages. *Energy Sources Part A Recov. Utilization Environ. Effects* **38**(14), 2035–2042. https://doi.org/10.1080/15567036.2015.1030477 (2016).
23. Qu, D. & Shi, H. Studies of activated carbons used in double-layer capacitors. *J. Power Sources* **74**(1), 99–107. https://doi.org/10.1016/S0378-7753(98)00038-X (1998).
24. Burke, A. R&D considerations for the performance and application of electrochemical capacitors. *Electrochim. Acta* **53**(3), 1083–1091. https://doi.org/10.1016/j.electacta.2007.01.011 (2007).

25. Sharma, P. & Bhatti, T. A review on electrochemical double-layer capacitors. *Energy Convers. Manage.* **51**(12), 2901–2912. https ://doi.org/10.1016/j.enconman.2010.06.031 (2010).

26. Momodu, D. *et al.* Transformation of plant biomass waste into resourceful activated carbon nanostructures for mixed-assembly type electrochemical capacitors. *Waste Biomass Valorization* **10**(6), 1741–1753. https://doi.org/10.1007/s12649-017-0165-x (2017).

27. Su, X. *et al.* Superior capacitive behavior of porous activated carbon tubes derived from biomass waste-cotonier strobili fibers. *Adv. Powder Technol.* **29**(9), 2097–2107. https://doi.org/10.1016/j.apt.2018.05.018 (2018).

28. Tey, J. P., Careem, M. A., Yarmo, M. A. & Arof, A. K. Durian shell-based activated carbon electrode for EDLCs. *Ionics* **22**(7), 1209–1216. https://doi.org/10.1007/s11581-016-1640-2 (2016).

29. Tsubota, T., *et al.* Catalytic graphitization for preparation of porous carbon material derived from bamboo precursor and performance as electrode of electrical double-layer capacitor. *J. Electron. Mater.* **44**(12), 4933–4939. https://doi.org/10.1007/s11664-015-4106-9 (2015).

30. Tsubota, T. *et al.* Capacitance property of carbon material derived from starch mixed with guanidine phosphate as electrochemical capacitor. *J. Power Sources* **227**, 24–30. https://doi.org/10.1016/j.jpowsour.2012.11.042 (2013).

31. Chang, J. *et al.* Activated porous carbon prepared from paulownia flower for high performance supercapacitor electrodes. *Electrochim. Acta* **157**, 290–298. https://doi.org/10.1016/j.electacta.2014.12.169 (2015).

32. Tsubota, T., Hohshi, Y., Ohno, T. & Kumagai, S. KOH activation of solid residue of Japanese citron after extraction by microwave process and property as EDLC electrode. *J. Porous Mater.* **27**(3), 727–734. https://doi.org/10.1007/s10934-019-00855-2 (2020).

33. Tsubota, T. *et al.* Preparation of porous carbon material derived from cellulose with added melamine sulfate and electrochemical performance as EDLC electrode. *J. Electron. Mater.* **48**(2), 879–886. https://doi.org/10.1007/s11664-018-6799-z (2018).

34. Tsubota, T., Ishimoto, K., Kumagai, S., Kamimura, S. & Ohno, T. Cascade use of bamboo as raw material for several high value products: Production of xylo-oligosaccharide and activated carbon for EDLC electrode from bamboo. *J. Porous Mater.* **25**(5), 1541–1549. https://doi.org/10.1007/s10934-018-0567-6 (2018).

35. Nguyen, A. T. *et al.* Release kinetics of potassium from silica-rich fern-derived biochars. *Agron. J.* **112**(3), 1713–1725. https://doi.org/10.1002/agj2.20209 (2020).

36. Chen, M. *et al.* Preparation of activated carbon from cotton stalk and its application in supercapacitor. *J. Solid State Electrochem.* **17**(4), 1005–1012. https://doi.org/10.1007/s10008-012-1946-6 (2012).

37. Liu, X. *et al.* Net-like porous activated carbon materials from shrimp shell by solution-processed carbonization and H_3PO_4 activation for methylene blue adsorption. *Powder Technol.* **326**, 181–189. https://doi.org/10.1016/j.powtec.2017.12.034 (2018).

38. Reffas, A. *et al.* Carbons prepared from coffee grounds by H_3PO_4 activation: Characterization and adsorption of methylene blue and Nylosan Red N-2RBL. *J. Hazard. Mater.* **175**(1–3), 779–788. https://doi.org/10.1016/j.jhazmat.2009.10.076 (2010).

39. Prahas, D., Kartika, Y., Indraswati, N. & Ismadji, S. Activated carbon from jackfruit peel waste by H_3PO_4 chemical activation: Pore structure and surface chemistry characterization. *Chem. Eng. J.* **140**(1–3), 32–42. https://doi.org/10.1016/j.cej.2007.08.032 (2008).

40. Liu, H. *et al.* Preparation of activated carbon from lotus stalks with the mixture of phosphoric acid and pentaerythritol impregnation and its application for Ni(II) sorption. *Chem. Eng. J.* **209**, 155–162. https://doi.org/10.1016/j.cej.2012.07.132 (2012).

41. Girgis, B. S. & El-Hendawy, A. A. Porosity development in activated carbons obtained from date pits under chemical activation with phosphoric acid. *Microporous Mesoporous Mater.* **52**(2), 105–117. https://doi.org/10.1016/S1387-1811(01)00481-4 (2002).

42. Li, Y., Zhang, X., Yang, R., Li, G. & Hu, C. The role of H_3PO_4 in the preparation of activated carbon from NaOH-treated rice husk residue. *RSC Adv.* **5**(41), 32626–32636. https://doi.org/10.1039/C5RA04634C (2015).

43. Abdelnaeim, M. Y., Sherif, I. Y., Attia, A. A., Fathy, N. A. & El-Shahat, M. Impact of chemical activation on the adsorption performance of common reed towards Cu(II) and Cd(II). *Int. J. Miner. Process.* **157**, 80–88. https://doi.org/10.1016/j.minpro.2016.09.013 (2016).

44. Molina-Sabio, M. & Rodríguez-Reinoso, F. Role of chemical activation in the development of carbon porosity. *Colloids Surfaces A Physicochem. Eng. Aspects* **241**(1–3), 15–25. https://doi.org/10.1016/j.colsurfa.2004.04.007 (2004).

45. Guo, Y. & Rockstraw, D. A. Physical and chemical properties of carbons synthesized from xylan, cellulose, and Kraft lignin by H_3PO_4 activation. *Carbon* **44**(8), 1464–1475. https://doi.org/10.1016/j.carbon.2005.12.002 (2006).

46. Baccar, R., Bouzid, J., Feki, M. & Montiel, A. Preparation of activated carbon from Tunisian olive-waste cakes and its application for adsorption of heavy metal ions. *J. Hazard. Mater.* **162**(2–3), 1522–1529. https://doi.org/10.1016/j.jhazmat.2008.06.041 (2009).

47. Fan, L. *et al.* High electroactivity of polyaniline in supercapacitors by using a hierarchically porous carbon monolith as a support. *Adv. Func. Mater.* **17**(16), 3083–3087. https://doi.org/10.1002/adfm.200700518 (2007).

48. Scorsone, E., Gattout, N., Rousseau, L. & Lissorgues, G. Porous diamond pouch cell supercapacitors. *Diam. Relat. Mater.* **76**, 31–37. https://doi.org/10.1016/j.diamond.2017.04.004 (2017).

Acknowledgements

Author contributions

T.K.T. wrote the main manuscript text and measured the samples. T.T. and M.N.N. revised the main manuscript text, and prepared figures. S.T. performed the experiments of H_3PO_4 activation and measured the samples. N.T.M. and N.H.N. performed the experiments of carbonization and H_3PO_4 activation, and elemental analysis of the samples. All authors reviewed the manuscript.

Competing interests

The authors declare no competing interests.

Additional information

Supplementary information is available for this paper at https://doi.org/10.1038/s41598-020-77099-7.

Correspondence and requests for materials should be addressed to T.T. or M.N.N.

Reprints and permissions information is available at www.nature.com/reprints.

Publisher's note Springer Nature remains neutral with regard to jurisdictional claims in published maps and institutional affiliations.